Symmetry Breaking Via Global Bifurcations of Modulated Rotating Waves in Hydrodynamics

Jan Abshagen,[1] Juan M. Lopez,[2] Francisco Marques,[3] and Gerd Pfister[1]

[1]*Institute of Experimental and Applied Physics, University of Kiel, 24098 Kiel, Germany*
[2]*Department of Mathematics and Statistics, Arizona State University, Tempe, Arizona 85287, USA*
[3]*Departament de Física Aplicada, Universitat Politècnica de Catalunya, 08034, Barcelona, Spain*

(Received 12 July 2004; published 25 February 2005)

The combined experimental and numerical study finds a complex mechanism of Z_2 symmetry breaking involving global bifurcations for the first time in hydrodynamics. In addition to symmetry breaking via pitchfork bifurcation, the Z_2 symmetry of a rotating wave that occurs in Taylor-Couette flow is broken by a global saddle-node-infinite-period (SNIP) bifurcation after it has undergone a Neimark-Sacker bifurcation to a Z_2-symmetric modulated rotating wave. Unexpected complexity in the bifurcation structure arises as the curves of cyclic pitchfork, Neimark-Sacker, and SNIP bifurcations are traced towards their apparent merging point. Instead of symmetry breaking due to a SNIP bifurcation, we find a more complex mechanism of Z_2 symmetry breaking involving nonsymmetric two-tori undergoing saddle-loop homoclinic bifurcations and complex dynamics in the vicinity of this global bifurcation.

DOI: 10.1103/PhysRevLett.94.074501 PACS numbers: 47.20.Ky, 44.25.+f, 47.20.Lz, 47.27.Te

Bifurcation theory has long been a very useful tool in the analysis of complex nonlinear dynamics. Global bifurcations, such as homo- and heteroclinic connections, are known to play important roles in organizing dynamics that originate in local bifurcations, and nearby solutions typically include very-low-frequency states and chaos [1].

Symmetries alter the solution structure near a bifurcation. The simplest symmetry in physical systems is Z_2 reflection symmetry. Taylor-Couette flow between two concentric rotating cylinders provides a canonical physical system that has been instrumental in developments in nonlinear dynamics and equivariant dynamical systems. Studies of the influence of end walls [2] opened up new perspectives into the importance of Z_2 symmetry, not only in Taylor-Couette flow, but in many other equivariant problems as well. Gluing bifurcations (where a symmetric limit cycle splits into a pair of Z_2-conjugate limit cycles) have been found in Taylor-Couette flows [3]. Z_2 symmetry breaking via global bifurcations are also thought to be important in a variety of physical systems [4]. Global bifurcation dynamics are well known to be an integral piece of the puzzle for understanding the transition to turbulence.

In this Letter, we provide a comprehensive comparison between experiments, numerics, and theory of nonlinear dynamics involving global bifurcations of two tori in a real physical system of infinite dimension. We describe the complex dynamics associated with Z_2 symmetry breaking in Taylor-Couette flow that we have found both experimentally and numerically, including a saddle-node-infinite-period (SNIP) bifurcation of nonsymmetric limit cycles (rotating wave states) on a symmetric two-torus (quasiperiodic modulated rotating waves). This curve of SNIP bifurcations provides a global connection between the symmetric modulated rotating wave that arises from a Neimark-Sacker (NS_s) bifurcation of a symmetric rotating wave and the pair of nonsymmetric rotating waves that arise from a cyclic pitchfork (CP) bifurcation of the same symmetric rotating wave. Focusing in on the region where these three bifurcation curves (SNIP, NS_s, and CP) approach each other, rather than meeting at a point, the transition between the symmetric and the nonsymmetric states involves further complex dynamics. The pair of Z_2-conjugate rotating waves suffer Neimark-Sacker (NS_a) bifurcations and the resulting pair of Z_2-conjugate modulated rotating waves simultaneously undergo saddle-loop homoclinic (SLH) bifurcations resulting in the symmetric modulated rotating wave.

The experimental Taylor-Couette setup consists of a fluid (silicon oil of kinematic viscosity $\nu = 10.2 \pm 0.1$ mm^2/s) confined between two concentric cylinders. The outer cylinder and the top and bottom end walls are held fixed. A phase-locked loop (PLL) circuit controlled the angular velocity of the inner cylinder, Ω, to better than one part in 10^{-4} in the short term and 10^{-7} in the long term average. The inner cylinder of radius $r_i = 12.50 \pm 0.01$ mm was machined from stainless steel and the outer cylinder of radius $r_o = 25.00 \pm 0.01$ mm was made from optically polished glass. The fluid temperature was thermostatically controlled to 21.00 ± 0.01 °C. The distance between the end walls, L, is adjustable to within ± 0.01 mm. Using the gap $d = (r_o - r_i)$ as the length scale, the geometric parameters are the aspect ratio $\Gamma = L/d$ and the radius ratio $\eta = r_i/r_o$ (fixed at $\eta = 0.5$). The dynamic parameter is the Reynolds number $\mathrm{Re} = \Omega d r_i/\nu$. Laser Doppler velocimetry (LDV) was used for velocity measurements. See [5] for further details.

The three-dimensional Navier-Stokes equations, nondimensionalized with d and viscous time scale d^2/ν, are solved using a Galerkin spectral-projection scheme. Legendre polynomial bases in the radial and axial directions, with 48 and 96 modes, respectively, a Fourier basis with 20 modes in the azimuthal direction, and a time step of 2×10^{-5} were used. See [6] for further details.

The range of aspect ratios examined here is $\Gamma \in [3.00, 3.25]$. In this range, for Reynolds numbers $\mathrm{Re} \sim 300$, a steady axisymmetric flow exists, consisting of four Taylor cells that form two outgoing jets of angular momentum erupting from the boundary layer on the inner cylinder. Figure 1(a) shows the streamlines of this 2-jet state at $\mathrm{Re} = 330$ and $\Gamma = 3.0$, and Fig. 1(b) is a flow visualization of this state. For $\mathrm{Re} \gtrsim 400$, this 2-jet state undergoes a Hopf bifurcation, spawning a rotating wave $\mathrm{RW_s}$ with azimuthal wave number $m = 1$ [5]. Both SO(2) rotational symmetry about the axis and Z_2 midplane reflection symmetry are broken, but $\mathrm{RW_s}$ retains a spatial symmetry consisting of a combination of the midplane reflection with a rotation of π radians about the axis (since it is a rotating wave, the half-period rotation in space is equivalent to a temporal evolution with $T/2$, where T is the precession period) that generates a Z_2-symmetry group. Figures 1(c) and 1(d) show contours of the azimuthal velocity of $\mathrm{RW_s}$ in two meridional planes π radians apart, computed for $\mathrm{Re} = 700$ and $\Gamma = 3.0$, illustrating this symmetry. The oscillation amplitudes of the two outward jets are large and they oscillate in phase. $\mathrm{RW_s}$ is robust, exists, and is stable for a large parameter range $400 < \mathrm{Re} < 625$.

The local codimension-one bifurcations that a Z_2 symmetric limit cycle ($\mathrm{RW_s}$) can undergo are via a real Floquet multiplier $\mu = +1$ or a pair of complex conjugate Floquet multipliers $\mu = e^{\pm i\omega}$ crossing the unit circle. The period doubling bifurcation $\mu = -1$ is inhibited due to the presence of the Z_2 symmetry [7]. When Z_2 symmetry is broken, the $\mu = +1$ bifurcation is a pitchfork of limit cycles and a pair of (symmetrically related) nonsymmetric limit cycles ($\mathrm{RW_a}$) are born. In the Neimark-Sacker bifurcation ($\mathrm{NS_s}$), with $\mu = e^{\pm i\omega}$, a modulated rotating wave ($\mathrm{MRW_s}$) is born; this quasiperiodic solution evolves on a two-torus T_s^2, which is Z_2 symmetric, although the individual $\mathrm{MRW_s}$ on it are not.

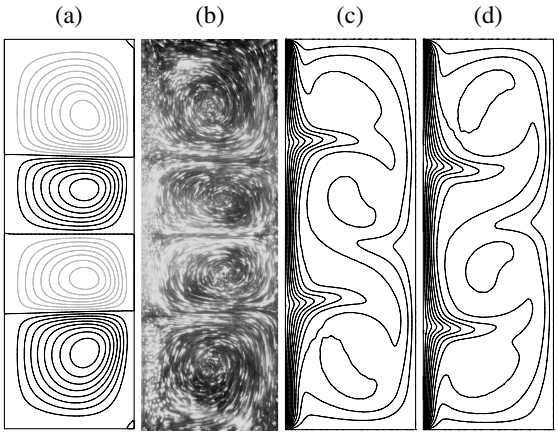

FIG. 1. (a) Computed streamlines and (b) flow visualization of the steady axisymmetric 2-jet state at $\mathrm{Re} = 330$, $\Gamma = 3.0$. (c), (d) Azimuthal velocity contours of $\mathrm{RW_s}$ at $\mathrm{Re} = 700$, $\Gamma = 3.0$ shown in two meridional planes π apart.

For $\mathrm{Re} > 640$ and increasing Γ beyond 3.18, $\mathrm{RW_s}$ suffers a cyclic pitchfork CP spawning a pair of $\mathrm{RW_a}$. For $\Gamma > 3.2$, CP is supercritical but becomes subcritical as $\Gamma \to 3.18$, spawning a pair of unstable $\mathrm{RW_a}$. These $\mathrm{RW_a}$ undergo saddle-node bifurcations with the pair of stable $\mathrm{RW_a}$ resulting from the CP at larger Γ. The stable and unstable manifolds of the $\mathrm{RW_a}$ are globally connected and the saddle-node bifurcation takes place on T_s^2; i.e., the saddle node is a global SNIP bifurcation. Following the SNIP, quasiperiodic $\mathrm{MRW_s}$ result. Continuing $\mathrm{MRW_s}$ to smaller Re and Γ, we find that $\mathrm{MRW_s}$ are spawned at a Neimark-Sacker bifurcation, $\mathrm{NS_s}$, from $\mathrm{RW_s}$. The loci of these three bifurcation curves in (Re, Γ) space are shown in Fig. 2; the solid (dotted) curves with filled (open) symbols were determined numerically (experimentally). The agreement between the two techniques is to within 1% (note that in the experiment the pitchfork is unfolded due to inherent small imperfections, and the curve shown is actually the saddle node from the disconnected branch of the imperfect pitchfork [2]).

As $\mathrm{MRW_s}$ approaches the SNIP bifurcation, its modulation period τ_s becomes infinite, following the typical $1/\text{square-root}$ law associated with saddle nodes. This behavior is illustrated in Fig. 3(a). The primary period, T, remains close to the precession period of $\mathrm{RW_s}$ from which it bifurcates, varying by about 10% over the parameter range considered here.

Figure 4(a) shows phase portraits [8] of $\mathrm{MRW_s}$ and $\mathrm{RW_a}$ [the two Z_2-conjugate states are shown in red/green (solid black)] on either side of the SNIP bifurcation. In order to illustrate the process of Z_2 symmetry breaking via the SNIP bifurcation, a one-parameter circuit in (Re, Γ) is followed (this path is shown in Fig. 2 by the star symbols):

$$\mathrm{RW_s} \xrightarrow{\mathrm{NS_s}} \mathrm{MRW_s} \xrightarrow{\mathrm{SNIP}} \mathrm{RW_a} \xrightarrow{\mathrm{CP}} \mathrm{RW_s}.$$

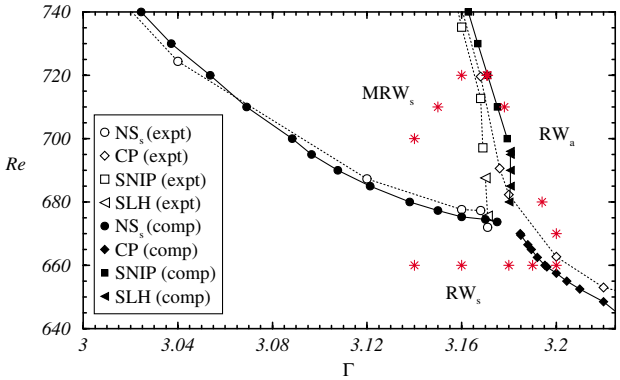

FIG. 2 (color online). Bifurcation curves in (Γ, Re) space; open (filled) symbols are determined experimentally (numerically). Stars indicate parameter values for Poincaré sections of the states shown in Fig. 4(b), for (Γ, Re) values (3.14, 660), (3.14, 700), (3.15, 710), (3.16, 720), (3.1705, 720), (3.171, 720), (3.178, 710), (3.194, 680), (3.2, 670), (3.2, 660), (3.19, 660), (3.18, 660), and (3.16, 660), clockwise from bottom left.

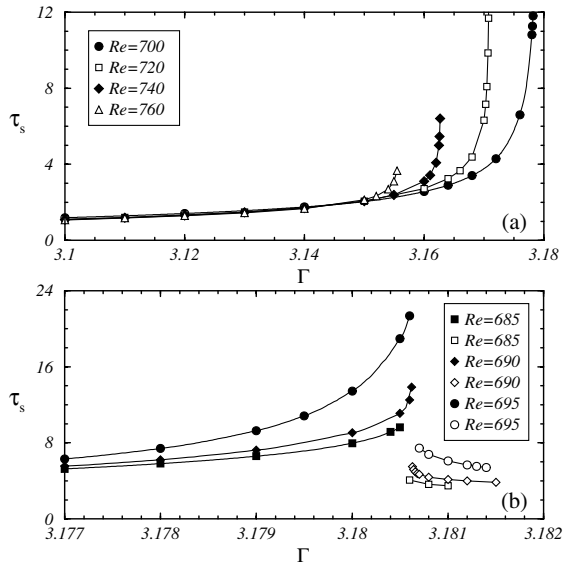

FIG. 3. Variation with Γ of (a) the modulation period of MRW_s near the SNIP bifurcation, and (b) the modulation periods of MRW_s (filled symbols) and MRW_a (open symbols) near the SLH bifurcation, computed for Re as indicated.

In order to gain further insight into the bifurcation process, Poincaré sections [9] of the solutions along the path are shown in Fig. 4(b). The path follows the symmetric rotating wave RW_s (open circles) undergoing a Neimark-Sacker bifurcation (NS_s) to a modulated rotating wave MRW_s (dotted curves). At onset, MRW_s has a near circular

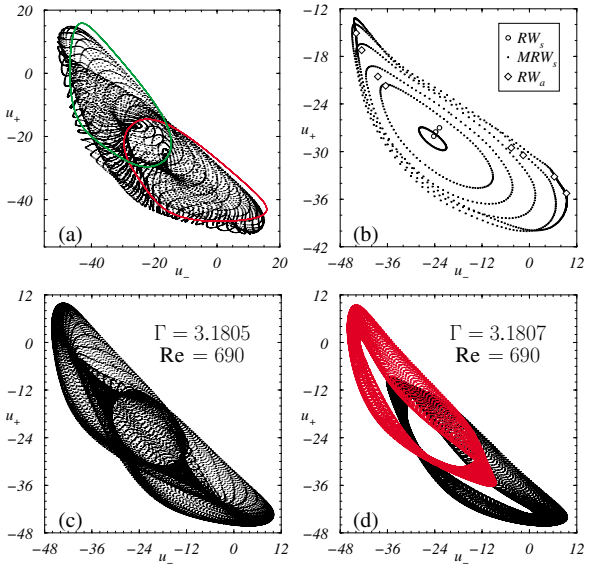

FIG. 4 (color online). (a) Computed phase portraits for MRW_s at Re = 720, Γ = 3.160 (black dots), and RW_a at Re = 720, Γ = 3.171 [red/green (solid black) curves for the conjugate states]. (b) Poincaré sections of states indicated by stars in Fig. 2. (c), (d) Computed phase portraits for MRW_s and MRW_a [Z_2-conjugate MRW_a in red (gray)].

Poincaré section which increases in radius as the distance from the bifurcation curve is increased. As MRW_s approaches the SNIP bifurcation curve, its section deforms and the iterates on the section accumulate about two opposite parts of the section, signaling the critical slowing down associated with the onset of saddle nodes on the section. At the SNIP bifurcation, a pair of saddle-node RW_a emerge on T_s^2, destroying it. On the other side of the SNIP bifurcation curve, we only show the Poincaré sections of the stable cycles, RW_a (open diamonds), as these are the ones we compute directly. As the path is followed towards the CP curve, the two Z_2-conjugate RW_a merge at the pitchfork, and we return to RW_s.

Focusing in on the region where the SNIP, NS_s, and CP bifurcation curves approach each other, we find that, rather than meeting at a point, there is instead a small window in parameter space where transition between the symmetric and the nonsymmetric states is accomplished via saddle-loop homoclinic (SLH) bifurcations. Figures 4(c) and 4(d) show phase portraits of the solutions found numerically in such a window. Note, in particular, the pair of Z_2-conjugate modulated rotating waves, MRW_a, in Fig. 4(d), which undergo SLH bifurcations with a pair of Z_2-conjugate saddle RW_a (resulting from the subcritical CP). Following the SLH bifurcation, the Z_2-symmetric MRW_s results [Fig. 4(c)]. The modulation periods of MRW_s and MRW_a grow unbounded following a log scaling law; see Fig. 3(b).

The Z_2-conjugate MRW_a arise from Neimark-Sacker bifurcations, NS_a, of the Z_2-conjugate RW_a; these bifurcations take place very close to the SLH bifurcations. The NS_a bifurcation curve is indistinguishable from the SLH bifurcation curve on the scale drawn in Fig. 2. Figure 5(a) is a zoomed in view of Fig. 2; the NS_a bifurcation curve and the SLH bifurcation curve are separated by ~0.03% variations in Γ.

Details of the bifurcation structure shown in Fig. 5(a) cannot be resolved with the present experimental apparatus. However, evidence is found that the global Z_2 symmetry-breaking bifurcation from MRW_s differs from a SNIP for lower Re in the experiments as well. Figure 6

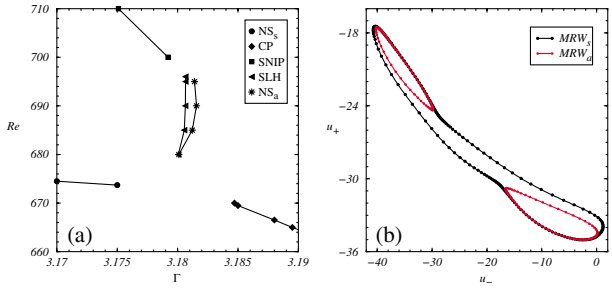

FIG. 5 (color online). (a) Close-up of the numerical bifurcation curves shown in Fig. 2. (b) Poincaré sections of MRW_s at Γ = 3.18062 and MRW_a at Γ = 3.18063, both at Re = 690 either side of the SLH bifurcation.

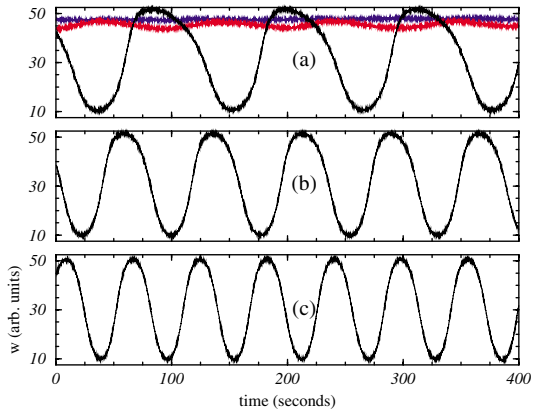

FIG. 6 (color online). Experimentally measured time series (in seconds) of the axial velocity at Re = 684.4 and (a) $\Gamma = 3.171$ (RW_a, blue), $\Gamma = 3.170$ (MRW_a, red), $\Gamma = 3.168$ (MRW_s, black), (b) $\Gamma = 3.166$ (MRW_s), and (c) $\Gamma = 3.162$ (MRW_s).

shows experimental time series of low-pass filtered axial velocity [10] measurements taken at $z = 0$ and $r = r_i + 1.5$ mm for Re = 684.4 for various Γ between 3.162 to 3.171. The time series for $\Gamma = 3.162$, 3.166, and 3.168 show the very-low-frequency oscillations of MRW_s whose modulation period grows rapidly as the global bifurcation is approached. The character of the time series at $\Gamma = 3.170$ is quite different, but there is still a very-low-frequency oscillation. This state is not space-time Z_2 symmetric; it is an MRW_a. At $\Gamma = 3.171$, the time series is essentially flat (aside from small amplitude fluctuations due to experimental noise), and the flow state corresponds to RW_a. Table I provides the underlying precession frequencies of all these states as well as the very-low (modulation) frequencies of the MRW. These results provide experimental evidence that the SLH scenario found numerically is physically robust, even though the details are not fully resolved experimentally.

Figure 5(b) shows Poincaré sections of the computed MRW_s and MRW_a at Re = 690, following a path in Γ across the SLH bifurcation. Notice that the Poincaré section of MRW_s becomes distorted into an oblique elliptical shape with the critical slowing down noted earlier occurring at the tips of the ellipse, and that as it approaches the SLH bifurcation, the minor axis of the ellipse collapses and the section takes on a figure-8 shape. Inside the small parameter window being considered, the collapse into the figure-8 shape of the section occurs before the critical slowing down at the tips of the section develop saddle nodes. Crossing the SLH bifurcation curve, the MRW_s section pinches off into two separate sections, corresponding to the Z_2-conjugate MRW_a.

This phenomenon, which we have been describing as the SLH bifurcations, is not a single event, but rather a complicated bifurcation process. There is actually an infinite series of bifurcations involving homoclinic structures as the stable and unstable manifolds of the saddle RW_a intersect transversally. This implies the existence of very-low-frequency states appearing and disappearing via saddle-node bifurcations, on a scale in parameter space which is not resolvable experimentally or numerically.

TABLE I. Frequencies (in Hz), of the flow states in Fig. 6.

Γ	Very-Low Frequency (Hz)	Precession Frequency (Hz)
3.162	0.0171	4.0039
3.166	0.0134	4.0040
3.168	0.0085	4.0039
3.170	0.0093	4.0035
3.171	⋯	4.0054

Symmetries and symmetry breaking are the most general organizing principles in modern physics, successfully applied in many areas of condensed matter physics including hydrodynamics. In this comprehensive comparison between precise experiments and numerical calculations of the Navier-Stokes equations, we have studied novel symmetry breaking and global bifurcations of time-dependent flows in a canonical hydrodynamic system. These new results on global bifurcations in hydrodynamics may provide a further piece in the puzzle for the understanding of the transition to turbulence.

[1] M. C. Cross and P. C. Hohenberg, Rev. Mod. Phys. **65**, 851 (1993); P. Glendinning and C. Sparrow, J. Stat. Phys. **35**, 645 (1984); T. Mullin and T. J. Price, Nature (London) **340**, 294 (1989).
[2] T. B. Benjamin, Proc. R. Soc. London A **359**, 1 (1978); **359**, 27 (1978); T. Mullin, J. Fluid Mech. **121**, 207 (1982).
[3] J. M. Lopez and F. Marques, Phys. Rev. Lett. **85**, 972 (2000); J. Abshagen, G. Pfister, and T. Mullin, *ibid.* **87**, 224501 (2001).
[4] S. P. Meacham, J. Phys. Oceanogr. **30**, 269 (2000); E. Simonnet *et al.*, *ibid.* **33**, 729 (2003); A. Algaba *et al.*, Int. J. Bifurcation Chaos Appl. Sci. Eng. **10**, 291 (1999); P. Glendinning, J. Abshagen, and T. Mullin, Phys. Rev. E **64**, 036208 (2001).
[5] U. Gerdts *et al.*, Phys. Rev. E **49**, 4019 (1994); J. von Stamm *et al.*, *ibid.* **54**, 4938 (1996).
[6] J. M. Lopez, F. Marques, and J. Shen, J. Comput. Phys. **176**, 384 (2002).
[7] J. W. Swift and K. Wiesenfeld, Phys. Rev. Lett. **52**, 705 (1984).
[8] The radial velocity $u_\pm$ is computed at two points, $p_\pm = (r = (r_0 + r_i)/2(r_0 - r_i), z = \pm 0.5\Gamma)$.
[9] The Poincaré section used is $w_+ + w_- = 0$, where $w_\pm$ are the axial velocities at $p_\pm$. The projection is onto $u_\pm$.
[10] A low-pass filter with cutoff at 0.5 Hz was used to filter out the precession frequency.